Numerical Modeling of Space Plasma Flows: ASTRONUM-2011
ASP Conference Series, Vol. 459
N. V. Pogorelov, J. A. Font, E. Audit, and G. P. Zank, eds.

Modeling of Solar Active Region Using a Three-Dimensional, Time-Dependent, Data-Driven Magnetohydrodynamic Model

S. T. Wu,[1,2] A. H. Wang,[1] David Falconer,[1] Qiang Hu,[1] Yang Liu,[3] Xueshang Feng,[4] and Fang Shen[4]

[1]*Center for Space Plasma and Aeronomic Research, The University of Alabama in Huntsville, Huntsville, AL 35899 USA*

[2]*Department of Mechanical and Aerospace Engineering, The University of Alabama in Huntsville, Huntsville, AL 35899 USA*

[3]*W.W. Hansen Experimental Physics Laboratory, Stanford University, Stanford, CA 99305 USA*

[4]*SIGMA Weather Group, State Key Lab of Space Weather, Center for Space Science and Applied Research, Chinese Academy of Sciences, PO Box 8701, Beijing 100190, China*

Abstract. A self-consistent, three-dimensional magnetohydrodynamic model together with time-dependent boundary conditions based on the method of characteristics at the bottom boundary (photosphere) to accommodate the observation will be discussed. To illustrate this model, Active Region 11117 observed by SDO/HMI is chosen for the analyses in that the magnetic field structures and evolution of this active region will lead to the determination of the conditions for the initiation of a solar eruption. Specific physical parameters to be simulated are non-potential magnetic field properties (i.e. emergence of magnetic flux (ϕ), the length of magnetic shear of the main neutral line (L_{ss}), and the total current helicity (H_c) injected into the corona). We have found that all the non-potential magnetic field properties are necessary conditions for a solar eruptive event, but a sufficient condition is revealed for AR11117 similar to the AR 10720 given by Wu et al. (2009). This sufficient condition is the "fragmentation" of the magnetic shear along the neutral line.

1. Introduction

It is very well recognized that the solar eruptions (i.e. flares and coronal mass ejections (CMEs)) will have significant adverse effects on the Earth's environment. These serious effects are the interruption of communication and possibly damaged power grids (Pirjola, 2007), the safety of astronauts, and the operation of space assets. Then, the important question to be asked is whether there is a possibility of predicting the occurrences of these solar eruptions. This issue has been with the solar community for years. The recent space mission such as SDO/HMI and HINODE have made high resolution and high cadence measurements of solar magnetic fields which provide a great opportunity to reveal the physical processes for solar eruptions.

Solar eruptive events have two main components, the coronal mass ejection (CME) and the flare. The CME typical properties consist of 10^{14-15} grams of mass ejected with velocities of 20 - 2500 km s^{-1}, total energy of up to 10^{31-32} ergs. An earthward directed CME can cause geomagnetic storms, a form of space weather 1 to 4 days after eruption. The flare emits strongly in the X-rays and can affect the ionosphere. In addition, the solar eruptive event can accelerate high energy particles, creating a solar energetic particle (SEP) event, which can arrive in Earth space tens of minutes after the flare. CME frequency depends on the solar cycle and can vary from 1 every 3 days to 3 a day. They erupt from highly magnetic sheared regions, with the worst tending to erupt from active regions. One way to improve forecast of them is to understand the evolution of the magnetic field properties of the source active region. The magnetic properties to investigate are the magnetic shear, the total magnetic flux, the net current, and the field twist as introduced by Falconer et al. (2002). Recently, Wu et al. (2009) analyzed AR 10720 and found an additional feature that main neutral line where the eruption occurred showed a fragmentation of the strong shear, (i.e. the degree of shear under the eruption was nonuniform). In this study, we will apply a data-driven active region evolution model to AR 11117 to explore these characteristics by studying the change of magnetic properties on the solar surface of the active region.

A description of the simulation model is given in §2, a brief description of observed AR 11117 in §3, and the numerical results are presented in §4. Finally the summary is given in §5.

2. Description of the Magnetohydrodynamic (MHD) Active Region Evolution Model

The mathematical model appropriate for the physical scenario we have referenced in the previous section can be expressed by a set of compressible, resistive magnetohydrodynamic (MHD) equations identical to those given by Wu et al. (2006). This set of governing equations consists of conservation of mass, momentum, energy and the induction equation. The induction equation accounts for non-linear dynamic interactions of plasma flow and magnetic field which produce the complex features in the solar atmosphere. For completeness, we repeat these governing equations as follows:

$$\frac{\partial \rho}{\partial t} + \nabla \cdot (\rho \mathbf{u}) = 0 \tag{1}$$

$$\rho\left(\frac{\partial \mathbf{u}}{\partial t} + \mathbf{u} \cdot \nabla \mathbf{u}\right) = -\nabla p + \frac{1}{4\pi}(\nabla \times \mathbf{B}) \times \mathbf{B} + F_g - 2\rho\omega_o \times \mathbf{u} - \rho\omega_o \times (\omega_o \times r) + \Psi,$$

where

$$\Psi = -\frac{2}{3}\nabla(\mu_t \nabla \cdot \mathbf{u}) + \mu_t[\nabla^2 \mathbf{u} + \nabla(\nabla \cdot \mathbf{u})] + 2[(\nabla \mu_t) \cdot \nabla]\mathbf{u} + [(\nabla \mu_t) \times (\nabla \times \mathbf{u})]; \tag{2}$$

$$\frac{\partial p}{\partial t} + \mathbf{u} \cdot \nabla p + \gamma p \nabla \cdot \mathbf{u} = (\gamma - 1)\nabla \cdot Q + (\gamma - 1)[\eta J^2 + \frac{\mu}{2}(\nabla \cdot \mathbf{u})^2]; \tag{3}$$

$$\frac{\partial \mathbf{B}}{\partial t} = \nabla \times (\mathbf{u} \times \mathbf{B}) + \lambda(\nabla \times \mathbf{B}) + \eta \nabla^2 \mathbf{B}. \tag{4}$$

In these equations, ρ is the plasma mass density, $\mathbf{u}$ is the plasma flow velocity vector, p is the plasma thermal pressure, $\mathbf{B}$ is the magnetic induction vector, $\mathbf{J}$ is the electric current and Q is the heat conduction. The other quantities are defined as follows: ω_o is the angular velocity of solar differential rotation referring to the center of the solar coordinate system given by Snodgrass (1983). The meridional flow profile used here is given by Hathaway (1996). F_g is the gravitational force, and γ, μ, λ, and η are the specific heat ratio (1.05), the viscosity, and the coefficients of cyclonic turbulence and effective diffusion. Finally, Ψ represents the viscous dissipation. This set of governing equations include the inertial coriolis force (i.e. $2\ \rho\omega_o \times \mathbf{u}$) and the centrifugal force ($\rho\omega_o \times (\omega_o \times r)$) due to the Sun's differential rotation in Eq. (2). The terms $\eta\nabla^2\ \mathbf{B}$ and $\lambda(\nabla \times \mathbf{B})$ in Eq. (4) represent the effective diffusion due to random motion of granules or supergranules and the cyclonic turbulence effect, respectively.

2.1. Initial and Boundary Conditions

To seek a numerical solution for Eqs (1) - (4) in the previous section, we have cast the set of governing equations in a rectangular coordinate system. The computational domain includes six planes (i.e. four side planes, plus top and bottom). Thus, it requires prescribing boundary conditions on these six planes. Because of the dominant features of the active region, we assume that the properties inside the active region will propagate outward and will not be affected by the properties outside the active region except the bottom boundary, thus the linear extrapolation is used for the top and four side planes. In order to accommodate the time-sequence of the photospheric measurements and realization of the set of governing equations being an initial boundary value problem (Courant and Hilbert, 1953), the set of governing Partial Differential Equations (PDEs) cover from elliptic to hyperbolic types of PDEs, and the flow regimes are in the range from subsonic, sub-Alfvenic to supersonic, super-Alfvenic. In order to assure the self-consistency, the method of projected characteristics originated by Nakagawa, Hu, and Wu (1987), and Wu and Wang (1987) will be used for the derivation of bottom boundary conditions. The detailed derivation and its resulted time-dependent boundary conditions are given in Wu et al. (2006) which will not be repeated here. Since the plasma flow near photosphere is sub-sonic and sub-Alfvenic, in accordance with the characteristics theory, it allows us to prescribe 5 out of 8 physical variables ($\mathbf{B}, \mathbf{u}, \rho, T$). The other 3 will be computed from compatibility equations (see Appendix, Wu et al. 2006).

To implement this evolutionary simulation of the active region, there are two steps; (i) establish a MHD equilibrium state as an initial state by using the photospheric measurements as the part of bottom boundary conditions, and (ii) seeking the evolution states of the active region using time-sequence of the photospheric measurements as the part of bottom boundary conditions (see Fig. 1). It should be noted from Figure 1 that this numerical code can be used for obtaining MHD equilibrium and evolution state, respectively.

2.1.1. Establishing Observationally the MHD Equilibrium State

To obtain the magnetohydrodynamic equilibrium state which represents the initial state based on the observed quantities as the part of boundary conditions for the evolutionary study comprises three steps: (a) to construct a trial 3D magnetic field configuration by using pre-event magnetograms together with non-force-free model by Hu et al (2010), or potential field model if the vector magnetogram is not available, (b) to prescribe den-

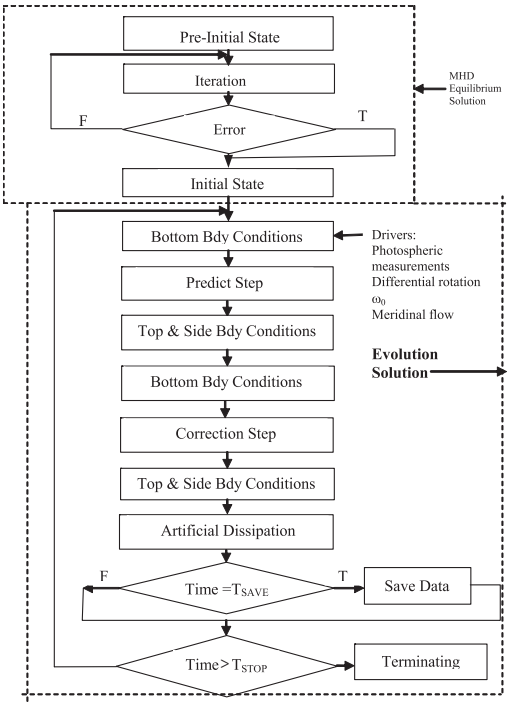

Figure 1. Computational Flow Chart for the 3D MHD code where 'F' and 'T' represent the "false" and "true," respectively. Note the upper box represents the code to compute the equilibrium solution and the lower box is for computing the evolutionary solution

sity distribution since there are no density measurements on the photosphere yet. The assumed trial valules are used (see Wu et al 2006) and (c) submitting the values given in (a) and (b) to the governing equations using the relaxation technique (Steinolfson, et al. 1982; Roache, 1998). The equilibrium state will be obtained for any trail values of the magnetic field, density and temperature. The criterion for the equilibrium state is $|\ (\Psi^{t+1} - \Psi^t)/\Psi^t\ | < \varepsilon$, where Ψ is physical parameters, and ε is an error measure. If the trail values are close to the equilibrium state, then the final equilibrium solution would rapidly converge to the equilibrium state.

2.1.2. Evolution of the Active Region Using Photospheric Measurements

To evolve the active region, we will input the photospheric measurements according to time-dependent bottom boundary conditions. For example, the magnetic field variation at the bottom boundary is described by a set of magnetograms. If the time cadence of the set is the same or smaller than the time step of the numerical code (CFL condition) then,

$$\mathbf{B}_{\text{bottom}}(x, y, t) = \mathbf{B}_{ob}(x, y, t) \tag{5}$$

If the time cadence is larger than the time step of the numerical code, then between two consecutive magnetogram values, for each numerical time step, we assume the linear

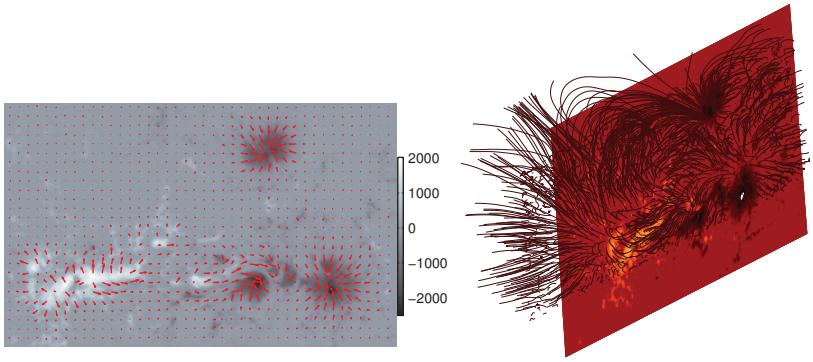

Figure 2. *Left panel*: Measured magnetic fields using HMI (Helioseismical Magnetic Imager) on-board SDO (Solar Dynamics Observatory) for AR11117, 2010 Oct 25, 22:00 UT. The arrows represent the transverse field and the gray scale indicates the intensity of the radial field (units in Gauss). *Right panel*: The simulated 3D magnetic field configuration of AR 11117, 2010 Oct 25, 22:00 UT using the input shown in the left panel

variation from one magnetogram to the next. For example, the magnetogram cadence is p min, and the time step is q sec, then

$$\mathbf{B}_{\rm bottom}(x,y,t) = \mathbf{B}_{ob}(x,y,t_n) + k\frac{\mathbf{B}_{ob}(x,y,t_{n+1}) - \mathbf{B}_{ob}(x,y,t_n)}{60p/q}, k = 1,2,...\frac{60p}{q}, \quad (6)$$

where $\mathbf{B}_{ob}$ is the measured magnetic fields, and subscript "n" represents the cadence of the magnetogram. The magnetograms are deprojected and their ambiguity is resolved using Metcalf methods (Metcalf 1994) and Gary et al (1987) which is based on a minimum energy solution (i.e. potential field model). For other accessible measurements (i.e. density, velocity, and temperature) a similar expression to Eq. (6) applies.

2.2. Numerical Techniques

The numerical scheme used for this code is the classical Total Variation Diminishing (TVD) Lax–Friedrich formulation (Toth and Odstricil 1996). This scheme is able to achieve dependent variable solutions, "temporally and spatially," to second order accuracy which is important to limit numerical error for physical realistic solution. To achieve the second order temporal accuracy, the Hancock predictor and corrector step (Yee, 1989) are used. The divergence clearing procedure given by Powell (1994) is also implemented in the code to assure satisfactory of the solenoidal condition. A computational flow diagram, that follows the initialization procedure described in §2.1.1, is given in Figure 1.

3. Description of NOAA AR 11117

Active Region NOAA AR11117 was recorded by SDO/HMI and H-alpha when it first appeared on 2010 Oct 20 near the east limb. It is a fast evolving AR because of the

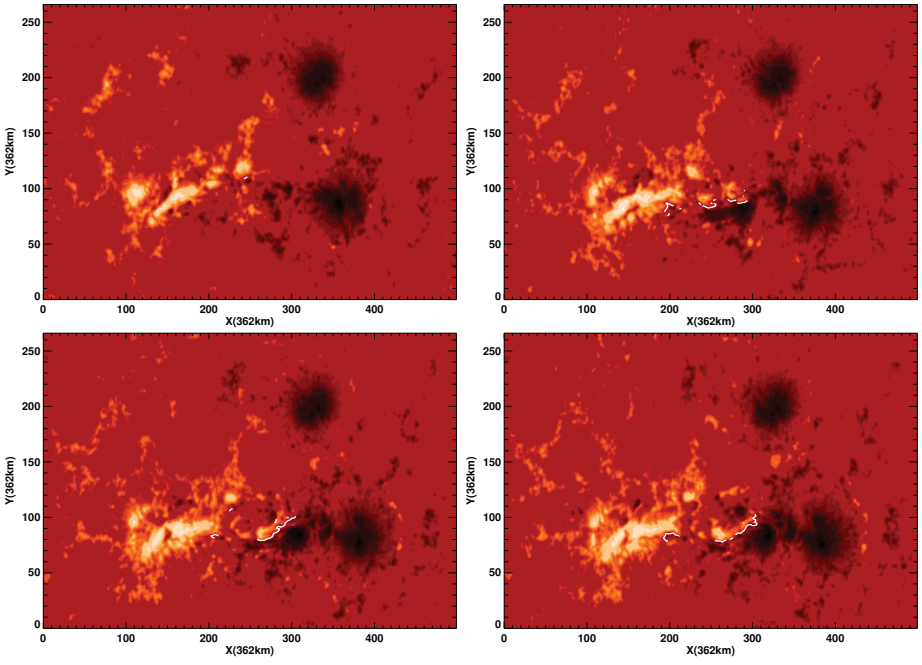

Figure 3. The simulated evolution of the length of strong magnetic shear of the main neutral line of AR 11117, 2010 Oct 25, at 00:00 UT (upper left), 14:00 UT (upper right), 19:00 UT (lower left), and 22:00 UT (lower right). Note the white line represent the portions of the neutral line that has strong magnetic shear (> 45°). The shear is the angle between the actual and potential magnetic field in the plane of the solar surface.

magnetic flux emerging during the period 2010 Oct 21-29, which triggers the photospheric surface dynamo. A confined C-2 flare occurred around 22:10UT on 2010 Oct 25. Figure 2 (left panel) shows the transverse field (arrows) and vertical field intensity measured by HMI on board SDO. In this study, we will focus our simulation in and around this time period. The simulation results are given in the next section.

4. Simulation Results

Following the procedures outlined in §2, we input the measured three components of magnetic field of AR11117 (see Fig. 2 (left panel)) together with assumed density distribution and constant temperature (10^5 K) to seek MHD equilibrium state. Using these simulated magnetic field, velocity field, density and temperature, we are able to construct the physical parameters discussed as follows: Figure 2 (right panel) shows the 3D magnetic field configuration at 22:00 UT, 2010 Oct 25. It exhibits the complexity of fields which is classified as the Beta-gamma region by Big Bear Solar Observatory (BBSO). The amount of free magnetic energy has reached up to $\sim 1.2 \times 10^{32}$ ergs which possesses the energy of a typical flare. It is worth noting that a C-2 flare appears at 22:10UT. Figure 3 shows the buildup of the strong magnetic shear length during day of Oct 25. The strong magnetic shear length is defined by the length having a shear

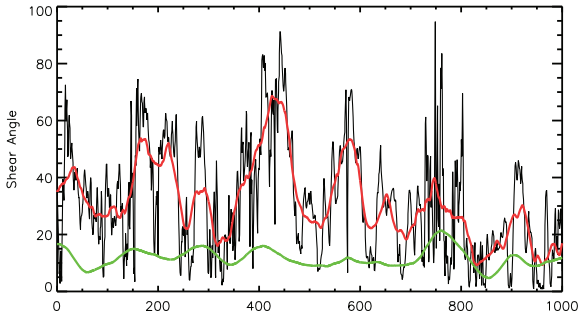

Figure 4. The variation of the shear angle along the fragmented neutral line (Fig 2) for AR11117, 2010 Oct 27 14:00 UT. The red line shows the spatial average of the shear angle (40" smoothing), and the green line is the standard deviation of the shear angle during the period of the day

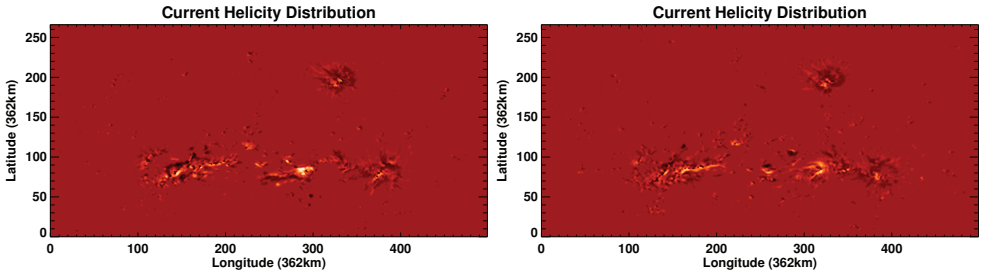

Figure 5. The simulated current helicity of AR11117 at 14:00 UT (left) and 22:00 UT (right), 2010 Oct 25.

angle larger than 45 ° and transverse field larger than 300 G (Falconer et al. 2002). It is clearly recognized that the magnetic shear length builds up step-by-step. At 22:00 UT the portions of the neutral line that has strong shear becomes fragmented in comparison to the previous time (19:00 UT). A C-2 flare occured at 22:10 UT. A similar feature was first simulated by Wu et al. (2009). To understand this fragmentation (or non-uniform) shear we use the measured magnetic field to construct the variation of the shear angle along the major neutral line as shown in Figure 4, which shows significant variation of the shear angle.

Finally, we show the change of total current helicity immediately before the observed C-2 flare in Figure 5 which shows an increasing swirling motion at the flaring location.

5. Summary

Recently, Wu et al (2009) found that before a major flare in AR 10720, the strong shear along the neutral line becomes fragmented. In this study, we use the same analysis method with a different active region (i.e. AR11117), and we found a similar fragmentation (i.e. a strong shear line feature also appeared as shown in Figure 3) which clearly indicates that the shear along the neutral line builds up until 19:00 UT, and then

becomes fragmented by 22:00 UT, and a C2 flare occurs at 22:10 UT. By looking at our simulation results including Fig. 5 which shows the increasing of the swirling motion of the current helicity near the flare site, we speculate that it could trigger the magnetohydrodynamic instability leading to final eruption. But we have not examined this feature fully yet, which will construe our future investigation.

Acknowledgments. The work performed by STW and AHW is supported by NSF ATM-0754378, NSF 0132798 via AURA SubAward C10569A, & NASA EPSCoR NNX09AP74A, DF is supported by MURI UCB154-4149 & NASA EPSCOR NNX-09AP74A, QH is supported by NASA grant NNX10AG03G, & NSF SHINE AGS-1062050. YL is supported by NAS5-02139 & NNH09CF22C, XF and FS are supported by the Natural Science Foundation of China and the Specialized Research Fund for State Key Laboratories (40921063, 40890162, 41031066, 40874077, 40874091, 41174150, & 41074121). The authors also wish to acknowledge the HMI team.

References

Courant, R. & Hilbert, D. 1953, in Methods of Mathematical Physics (New York: Interscience Publ. Inc.)
Falconer, D. A., Moore, R. L., & Gary, G. A. 2002, ApJ, 569, 1016
Gary, A. G., Moore, R. L., Haygard, M. J. & Haisch, B. M. 1987, ApJ, 314, 782
Hathaway, D. H. 1996, ApJ, 460, 1027
Hu, Q., Dasgupta, B., DeRosa, M.L., Büchner, J., & Gary, G.A. 2010, JASTP, 72, 219
Metcalf, T. R. 1994, Solar Phys., 115, 235
Nakagawa, Y., Hu, Y. Q., & Wu, S. T. 1987, Astron. Astrophys., 179, 354
Pirjola, R. 2007, in Space Weather - Physics and Effects, edited by V. Bothmer & I. Daglis (Berlin: Springer)
Powell, K. G. 1994, in A Reimann solver for ideal MHD that works in more than one dimension, ICASE Report No. 94-24, (Langley, VA)
Roache, P. J. 1998, in Fundamentals of Computational Fluid Dynamics, (Albuquerque: Hermosa Publisher,)
Snodgrass, H. R. 1983, ApJ, 270, 288
Steinolfson, R. S., Suess, S. T., & Wu, S. T. 1982, ApJ, 255, 730
Toth, G. & Odstrcil, D. 1996, J. Comput. Phys. 128, 82
Wu, S. T. & Wang, J. F. 1987, Computer Methods in Applied Mechanics and Engineering, 64, 267
Wu, S. T., Wang, A. H, & Falconer, D. A. 2005, in IAU Symp. 226, Coronal and Stellar Mass Ejections, edited by K. P. Dere & J. X. Wang (Cambridge: Cambridge Univ. Press)
Wu, S. T., Wang, A. H., Liu, Y., & Hoeksema, J. T. 2006, ApJ, 652, 800
Wu, S. T., Wang, A. H., Gary, G. A., Kucera, A., Rybak, J., Liu, Y., Vrsnak, B., & Yurchyshyn, V. 2009, Adv. Space Res., 44, 46
Yee, H. C. 1989, A class of high resolution explicit and implicit shock-capturing method, NASA TM-101088